SONIC COMPOSITES AS NOISE BARRIERS

LIGIA MUNTEANU, VETURIA CHIROIU, CIPRIAN DRAGNE, VALERIA MOȘNEGUȚU, NICOLETA NEDELCU, IULIAN GIRIP, CRISTIAN RUGINĂ

Abstract. We address an alternative road traffic noise barrier as a sonic composite consisted of an array of acoustic scatterers embedded in air. Acoustic scatterers are piezoceramic hollow spheres of functionally graded materials - the Reddy graded hollow spheres. Multiple (Bragg) scattering lead to a selective sound attenuation in the frequency bands called band gaps or stop bands for certain spacing and size of the scatterers. Size variations of the band gaps are discussed in this paper by taking into account the intrinsic acoustic properties of the scatterers. We reveal that the noise barrier simulation in the context of the road traffic noise confirm the Bragg band gaps existence and the predicted multiple resonances at frequencies below the first Bragg band gap.

Key words: Sonic composite, Band-gaps, Multiple resonances, Noise barrier.

1. INTRODUCTION

In the past few years, the accurate predictions of the interactions of acoustic waves with periodic structures show the potential of sonic composites to work as noise barriers in the road traffic noise [1–6]. According to the Bragg's theory, the sonic composites can generate large band-gaps from multiple reflected waves with large acoustic impedance ratios between the scatterers and the matrix, respectively [7–9]. The sonic composites are composed of scatterers embedded into air. The scatterers are local resonators which scater, diffuse or disperse energy, such as spheres, rods or cylinders. The sonic composite is the sonic version of the photonic crystal being architectured such that the sound is not allowed to propagate in certain full band-gaps due to complete reflections. Existence of the band-gaps makes this material the main candidate for applications as the acoustic filters [10], acoustic barriers [11] or wave guides [12, 13].

Many unique properties of the sonic composites come from the generation of large band-gaps at different frequencies inverse proportional to the central distance between two scatterers [14]. The band-gap generation mechanism means the

Institute of Solid Mechanics, Romanian Academy, Bucharest

Ro. J. Techn. Sci. – Appl. Mechanics, Vol. 65, N° 2, P. 123–136, Bucharest, 2020

completely reflected waves in the frequency range where all partial band-gaps overlap. This can be explained by evanescent waves [15] which lead to localized modes withe no real wave number [16, 17].

In the present paper, we investigate an alternative noise barrier as a 3D sonic composite with scatterers made from functionally graded materials with radial polarization [18–20].

Architectural acoustics deals with the sound quality of closed and open spaces [28]. Sound perception in the free field is different from halls because reflections on the walls are missing. In the free field, only the direct sound comes to the listener. When the space is closed, the sound gives rise to a multitude of reflections that decrease in time and space.

Unwanted noise is perceived as a dangerous factor for human health [21] and an environmental stressor in the road traffic especially during the night time in the urban areas [22, 23]. The extra low frequency band gaps in the sonic composites can be exploited in the noise barrier located above the ground surface as suggested in [3, 24] where cylindrical PVC embedded in air or arrangements of triangular, square or elliptical rigid scatterers (square lattice) were used for scatterers.

The efficiency of a barrier along the highways depends on the moving traffic and the vehicle type and velocity [28]. According to STAS 9783/1–94 Standard Acoustics in Constructions [29], the normalized traffic noise spectrum measured in A-weighted decibel (dBA) lies between 100 Hz to 5 KHz, with the main noise energy centred at 1 kHz. In addition, the normalized traffic noise spectrum does not take into accounts the temporal effects of the moving traffic. Efficiency of a road traffic noise barrier is measured by the *Insertion Loss* (IL) expressed in Decibel [dB] as

$$\mathrm{IL} = 20\log_{10}\left|\frac{p_{dir}}{p_{tr}}\right|, \tag{1}$$

where p_{dir} and p_{tr} denote the pressure obtain without and with the barrier, respectively.

Conventional attenuating of the traffic noise knows two main mechanisms highly frequency dependent. At the lower end of the frequency spectrum of interest (below 1 kHz) the ground effect is the most important mechanism. At the frequencies greater than 2 kHz, the noise can be attenuated by absorbing of the noise by leaf. In both cases, it was necessary to have planted vegetation belt to obtain a little attenuation.

Tree plantations arranged periodically can also attenuate the noise at low frequencies.

High attenuations at low frequencies (< 500 Hz) may occur by devices of destructive interference of the scattered waves. The research of the sonic composites barriers exploits the properties of the scatterers which scater, diffuse or disperse energy. The scatterers can be spheres, rods or cylinders. The noise barriers

made of the sonic composites offer an alternative mechanism of absorption, in addition to multiple scattering waves in the periodic structure. The influence of wind generated by the noise also affects the efficiency of the noise barrier. It was found that the adverse influence is absent up to wind speeds of 30 m/s [3].

The bandgap generation requires a large contrast in the density and velocity of sound between the scatterer and the matrix material. We show this in the following.

The acoustic impedance of a material Z, and the wave velocity v, are expressed as

$$Z = \rho v = \sqrt{E\rho}\,,\ v = \sqrt{\frac{K}{\rho}}\,, \tag{2}$$

where ρ, E and K are the density, the Young's elasticity modulus and bulk modulus of the material, respectively.

In a sonic crystal with square lattice, the fundamental Bragg resonance frequencies in the lattice main directions are separated by a factor of $\sqrt{2}$ as [3]

$$f_{Bragg,x} = \frac{c}{2l}\,,\ f_{Bragg,y} = \frac{c}{2l\sqrt{2}}\,, \tag{3}$$

where c is the speed of sound (344 m/s in air at room temperature 20ºC).

On the other hand, the hexagonal lattice the Bragg resonances are separated by $\sqrt{3}$ which result in a wider bandgap for a higher acoustic impedance mismatch between the matrix and the scatterer [3].

The nature of the matrix is the difference between the sonic and phononic crystals. If the matrix is solid then the term *phononic crystal* is used for the artificial crystal. The phononic crystals exhibit both longitudinal and transverse shear waves, but in contrast, the sonic crystals are independent of the transverse waves. The scatterers are made of solid materials and the matrix is air to obtain high acoustic impedance contrast between them.

2. THE SONIC COMPOSITE

The sonic composite discussed in this paper contains an array of 144 piezoceramic hollow spheres of functionally graded materials with diameter a and embedded in air. This panel is displayed in Fig.1. For simplicity, we consider all spheres are tangent to each other. The length of the panel is L, the width is d, and its thickness is $e = a$. The coordinate system $Ox_1x_2x_3$ is introduced with origin in

the middle plane of the plate, the axis Ox_1 in-plane normal to the layers and the axis Ox_3 out-plane normal to the plate.

Absorbing boundary conditions in the x_1-direction at $x_1 = 0$ and $x_1 = l$ have the role to avoid the unphysical reflections. The transducer send the plane monochromatic waves in the x_1-direction and the receiver measures the displacements at both sides of the plate at $x_1 = b$ and $x_1 = l - b$, respectively. The ratio of the displacement at the receiver and the input transducer, respectively measures the sound attenuation.

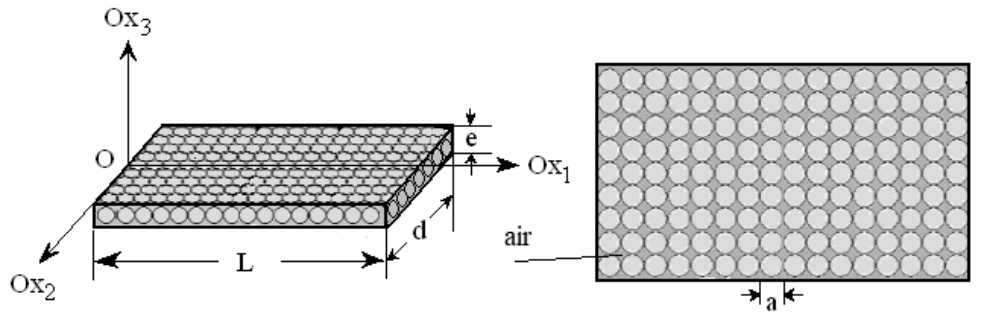

Fig. 1 – The sonic composite consisted of an array of acoustic scatterers embedded in air.

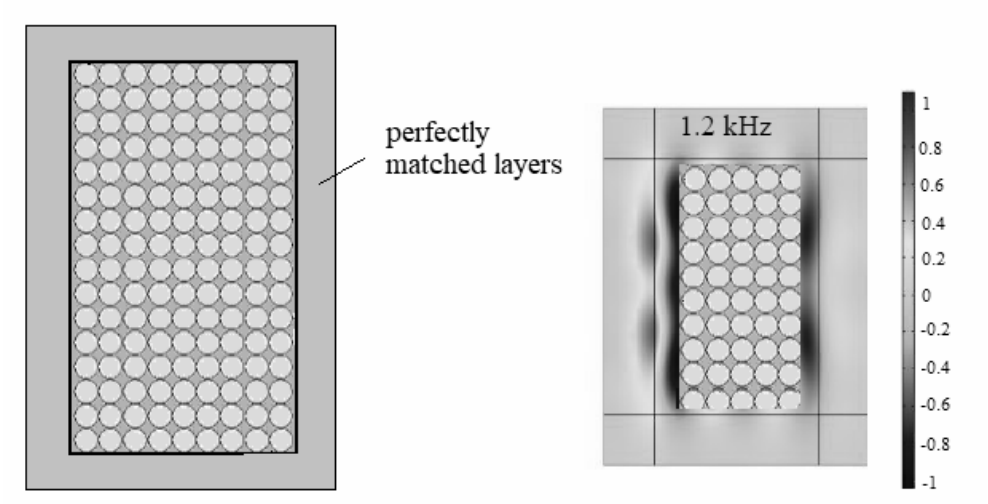

Fig. 2 – Artificial perfectly matched layers at the boundaries of the sonic composite; a) location of the layers; b) pressure map at 1.2 kHz computed by FEM.

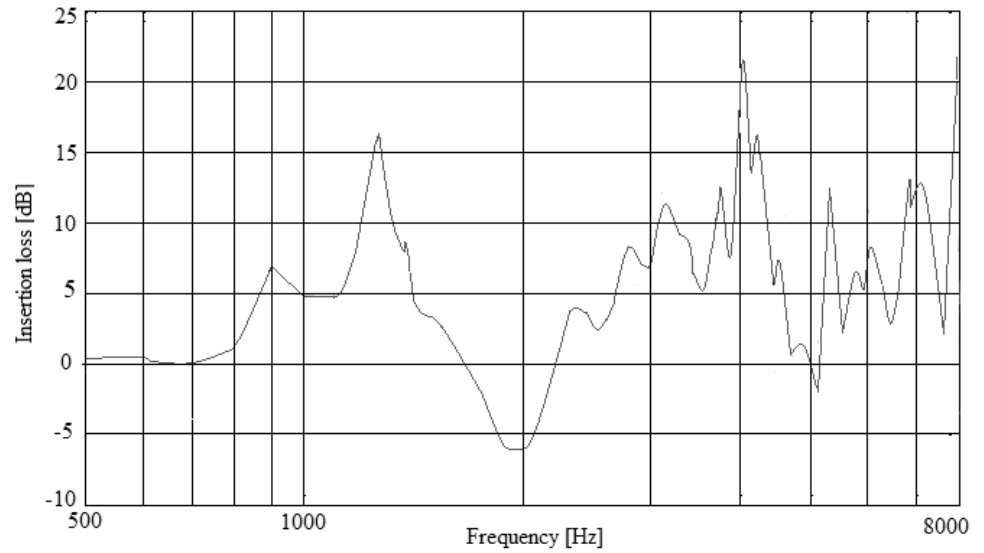

Fig. 3 – Insertion Loss with respect to the frequency computed by FEM.

The Sommerfeld condition of radiation means the absence of all reflection from the boundaries. To obtain an unbounded medium an artificial perfectly matched layers may to be introduced at the boundaries of the panel. In these layers, the wave equation contains a damping term which attenuates proportionally with distance in the direction perpendicular to the interface with the physical domain. Location of the perfectly matched layers at the boundaries of the panel is shown in Fig. 2a.

The pressure map computed by FEM for 1.2 kHz is presented in Fig. 2b. We see that the wave incident upon the layers is absorbed only in the outgoing direction, while the tangential waves to the interface between the layers and the physical domain remain unaffected. Important is that the wave incident upon these layers from environment do not reflect at the interface.

Figure 3 shows the variation of the Insertion Loss with respect to frequency. The panel is predicted to produce the highest amplitude Bragg band gap at 1.3 kHz. This suggests that much of the incoming wave front is blocked by the larger surface of the scatterer. Also, the Bragg band gap is predicted to contain two peaks instead of one.

The elastic, piezoelectric and dielectric constants depend on the radial coordinate r. The following notations are introduced: σ_{ij} the stress tensor, ϕ the electric potential, D_i the electric displacement vector, C_{ij} the elastic constants, $C_{66} = (C_{11} - C_{12})/2$, f_{ij} the piezoelectric constants f_{ij}, ζ_{ij} the dielectric constants, $i = r, \theta, \varphi$, and ρ the density of the material.

The constitutive equations for the piezoelectric hollow sphere in the spherical coordinate system (r,θ,φ) are given by [25–27]

$$r\sigma_{\theta\theta} = C_{11}S_{\theta\theta} + C_{12}S_{\varphi\varphi} + C_{13}S_{rr} + f_{31}r\phi_r\,,$$

$$r\sigma_{\varphi\varphi} = C_{12}S_{\theta\theta} + C_{11}S_{\varphi\varphi} + C_{13}S_{rr} + f_{31}r\phi_{,r}\,,$$

$$r\sigma_{rr} = C_{13}S_{\theta\theta} + C_{13}S_{\varphi\varphi} + C_{33}S_{rr} + f_{33}r\phi_{,r}\,,$$

$$r\sigma_{r\theta} = 2C_{44}S_{r\theta} + f_{15}\phi_{,\theta}\,,\ r\sigma_{r\varphi} = 2C_{44}S_{r\varphi} + f_{15}\csc\theta\phi_{,\varphi}\,, \tag{4}$$

$$r\sigma_{\theta\varphi} = 2C_{66}S_{\theta\varphi}\,,\ rD_\theta = 2C_{15}S_{r\theta} - \zeta_{11}\phi_{,\theta}\,,$$

$$rD_\varphi = 2f_{15}S_{r\varphi} - \zeta_{11}\csc\theta\phi_{,\varphi}\,,$$

$$rD_r = f_{31}S_{\theta\theta} + f_{31}S_{\varphi\varphi} + f_{33}S_{rr} - \zeta_{33}r\phi_{,r}\,.$$

The strain components ε_{ij} are related to the displacement components u_i, $i = r,\theta,\varphi$ by

$$r\varepsilon_{rr} = ru_{r,r}\,,\ r\varepsilon_{\theta\theta} = u_{\theta,\theta} + u_r\,,$$

$$r\varepsilon_{\varphi\varphi} = \csc\theta u_{\varphi,\varphi} + u_r + u_\theta\cot\theta\,,$$

$$2r\varepsilon_{r\theta} = u_{r,\theta} + ru_{\theta,r} - u_\theta\,,\ 2r\varepsilon_{r\varphi} = \csc\theta u_{r,\varphi} + ru_{\varphi,r} - u_\varphi\,, \tag{5}$$

$$2r\varepsilon_{\theta\varphi} = \csc\theta u_{\theta,\varphi} + u_{\varphi,\theta} - u_\varphi\cot\theta\,.$$

The electrostatic charge is described as

$$r(rD_r)_{,r} + rD_r + \csc\theta(rD_\theta\sin\theta)_{,\theta} + \csc\theta(rD_\varphi)_{,\varphi} = 0\,. \tag{6}$$

To simplify the motion equations, the Chen functions F, G and w, and the stress functions Σ_1 and Σ_2 are introduced [25–27]

$$u_\theta = -\csc\theta F_{,\varphi} - G_{,\theta}\,,\ u_\varphi = F_{,\theta} - \csc\theta G_{,\varphi}\,,\ u_r = w\,,$$

$$r\sigma_{r\theta} = -\csc\theta\Sigma_{1,\varphi} - \Sigma_{2,\theta}\,,\ r\sigma_{r\varphi} = \Sigma_{1,\theta} - \csc\theta\Sigma_{2,\varphi}\,. \tag{7}$$

Consequently, the motion equations can be written as two independent sets of equations

$$rA_{,r} = MA\,,\ rB_{,r} = PB\,, \tag{8}$$

$$B = [r\sigma_{rr}, \Sigma_2, G, w, rD_r, \phi]^T\,,$$
$$M = \begin{bmatrix} -2 & -C_{66}(\nabla^2 + 2) + r^2\rho\dfrac{\partial^2}{\partial t^2} \\ C_{44}^{-1} & 1 \end{bmatrix}, \tag{9}$$

where $\nabla^2 = \dfrac{\partial^2}{\partial\theta^2} + \cot\theta\dfrac{\partial}{\partial\theta} + \csc^2\theta\dfrac{\partial^2}{\partial\varphi^2}$. The matrix P has the components:

$$P_{11} = 2\beta - 1\,,\ P_{12} = \nabla^2\,,\ P_{13} = k_1\nabla^2\,,\ P_{14} = -2k_1 + r^2\rho\frac{\partial^2}{\partial t^2}\,,$$

$$P_{15} = 2P_{25} = -P_{64} = 2\gamma\,,\ P_{21} = \beta\,,\ P_{22} = -2\,,$$
$$P_{23} = k_2\nabla^2 - 2C_{66} + r^2\rho\frac{\partial^2}{\partial t^2}\,,\ P_{24} = -k_1\,,\ P_{32} = C_{44}^{-1}\,, \tag{10}$$
$$P_{33} = P_{34} = -P_{55} = 1\,,\ P_{36} = C_{44}^{-1}f_{15}\,,\ P_{41} = \alpha^{-1}\zeta_{33}\,,\ P_{43} = \beta\nabla^2\,,$$
$$P_{44} = -2\beta\,,\ P_{45} = \alpha^{-1}f_{33}\,,\ P_{52} = C_{44}^{-2}f_{15}\nabla^2\,,\ P_{56} = k_3\nabla^2\,,$$
$$P_{61} = \alpha^{-1}f_{33}\,,\ P_{63} = \gamma\nabla^2\,,\ P_{65} = -\alpha^{-1}C_{33}\,,$$

with

$$\alpha = C_{33}\zeta_{33} + f_{33}^2\,,\ \beta = \alpha^{-1}(C_{13}\zeta_{33} + f_{31}f_{33})\,,$$
$$\gamma = \alpha^{-1}(C_{13}f_{33} - C_{33}f_{31})\,,\ k_1 = 2(C_{13}\beta + f_{31}\gamma) - (C_{11} + C_{12})\,, \tag{11}$$
$$k_2 = 0.5k_1 - C_{66}\,,\ k_3 = \zeta_{11} + f_{15}^2C_{44}^{-1}\,.$$

The functionally graded material is described by the Reddy law [18–20]

$$M = M_p\mu^\lambda + M_z(1 - \mu^\lambda)\,, \tag{12}$$

where ξ_0 is the ratio of the inner and outer radii of the hollow sphere, μ is the gradient index, M_p and M_z are material constants of two materials, namely PZT-4 and ZnO. The case $\mu = 0$ corresponds to a homogeneous PZT-4 hollow sphere and $\mu \to \infty$, to a homogeneous ZnO hollow sphere.

Sharp periodic boundary conditions in displacement and traction are considered at the interfaces between the hollow spheres and air.

The sets of equations (8) imply two independent classes of free vibrations. The first class does not involve the piezoelectric or dielectric parameters, and corresponds to the isotropic elastic sphere. The second class depends on the piezoelectric and the dielectric parameters. When the gradient index μ increases, the natural frequencies increase for all modes.

The equations (8) – (12) are solved by the cnoidal method [8, 9].

3. NOISE BARRIER

The research objective of the paper is to use the sonic composite shown in Fig. 1 to design an outdoor noise barrier. Multiple independent resonance bandgaps below the first Bragg bandgap (due to the periodicity of the scatterers) between 400 and 1600 Hz are needed for the traffic noise.

The noise barrier is a 1×144 array of hollow piezoelectric ceramic hollow spheres of diameter $a=0.11\,\mathrm{m}$ embedded in air. The length of the plate is $L=1.76\,\mathrm{m}$ the width is $d=0.99\,\mathrm{m}$, and its thickness is $e=a=0.11\,\mathrm{m}$. The thickness of the hollow sphere is 0.00275m and $\xi_0=0.3$.

The numerical results are carried out for the following constants [2]:

- for PZT-4: $C_{11}=13.9\times10^{10}\,\mathrm{N/m^2}$, $C_{12}=7.8\times10^{10}\,\mathrm{N/m^2}$,

$$C_{13}=7.4\times10^{10}\,\mathrm{N/m^2},$$

$$C_{33}=11.5\times10^{10}\,\mathrm{N/m^2},\ C_{44}=2.56\times10^{10}\,\mathrm{N/m^2},\ f_{15}=12.7\mathrm{C/m^2},$$

$$f_{31}=-5.2\mathrm{C/m^2},\ f_{33}=15.1\mathrm{C/m^2},\ \zeta_{11}=650\times10^{-11}\,\mathrm{F/m},\ \zeta_{33}=560\times10^{-11}\,\mathrm{F/m},$$

$$\rho=7\,500\mathrm{kg/m^3};$$

for ZnO: $C_{11}=20.97\times10^{10}\,\mathrm{N/m^2}$, $C_{12}=12.11\times10^{10}\,\mathrm{N/m^2}$,

$$C_{13}=10.51\times10^{10}\,\mathrm{N/m^2},\ C_{33}=21.09\times10^{10}\,\mathrm{N/m^2},\ C_{44}=4.25\times10^{10}\,\mathrm{N/m^2},$$

$$f_{15}=-0.59\mathrm{C/m^2},\ f_{31}=-0.61\mathrm{C/m^2},\ f_{33}=1.14\mathrm{C/m^2},$$

$$\zeta_{11}=7.38\times10^{-11}\,\mathrm{F/m},\ \zeta_{33}=7.83\times10^{-11}\,\mathrm{F/m},\ \rho=5\,676\mathrm{kg/m^3},\ \mu=0.5;$$

and for air $\rho_{air}=1.2\,\mathrm{kg/m^3}$ and speed of sound is $344\ \mathrm{ms^{-1}}$.

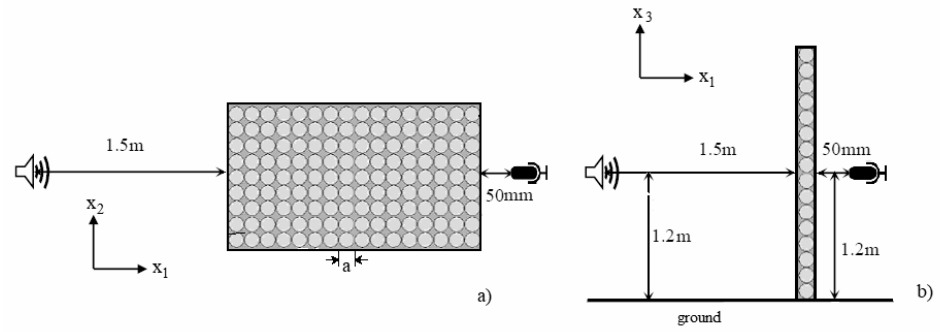

Fig. 4 – a) Plan view of the noise barrier; b) side view of the noise barrier.

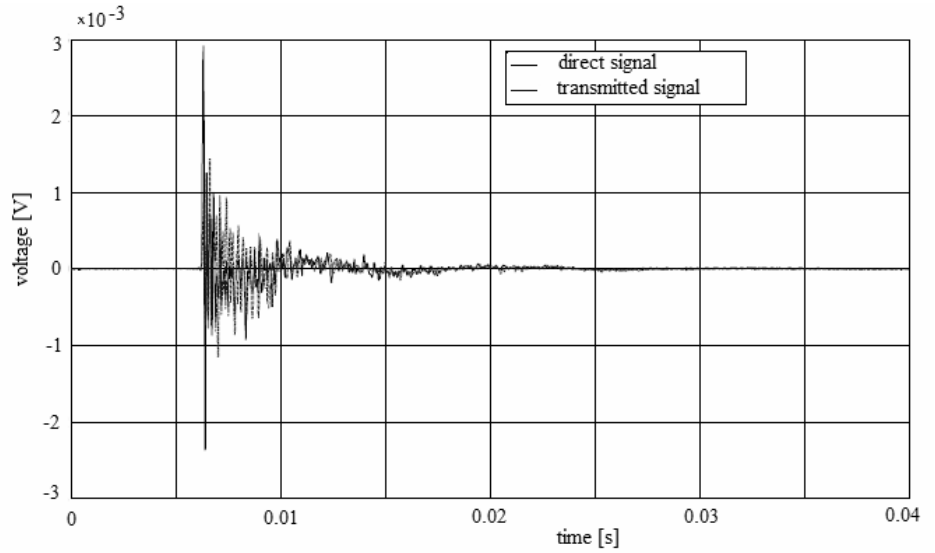

Fig. 5 – Direct and the transmitted signals variation with respect to time.

We assume that the receiver microphone is located at 50 mm from the opposite face of the source. The source and receiver are located at 1.2 m above the ground. The loud speaker is placed between 1.5 m and 1.63 m away from the barrier such that the source-receiver axis is normal to the barrier orientation Fig. 4.

The input signal is simulated by removing any signals with frequency beyond the 10 kHz.

Figure 5 shows the time signals corresponding to the direct and transmitted fields of signals through the barrier.

Figure 6 plots the dispersion curve including the first partial band-gaps for the sonic composite. The reduced units for the frequency are $\omega a / 2\pi c_0$, with c_0 the speed of sound in air.

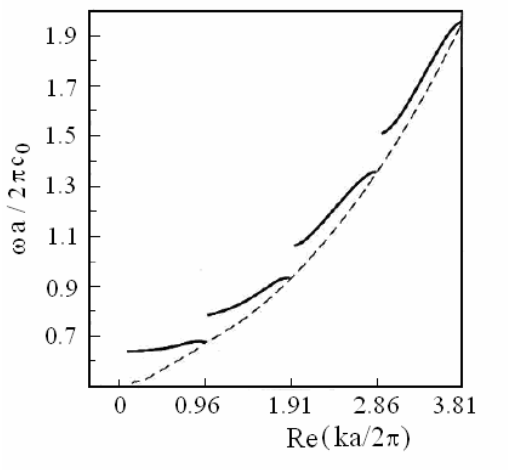

Fig. 6 – Linear dispersion for panel.

The guided waves are accompanied by evanescent waves which extend to the periodic array of the scatterers surrounding the wave-guide. Using the Joannopoulus theory of the bad-gap structure [14], Fig. 7 presents the band structure with the evanescent modes with exponential decay. The central grey region is the full band-gap ranged between 8.02 kHz and 8.72 kHz, given by the real part of the wave vector constrained in the first Brillouin zone for each frequency. The left region shows the imaginary part of the wave vector for longitudinal direction frequency, while the right region is the imaginary part of the wave vector for transverse direction frequency. The red lines represent the imaginary part of the wave vector of the evanescent modes inside the bad-gap.

A full band-gap can be obtained by adding band-gaps for both longitudinal and transverse waves in the same frequency region.

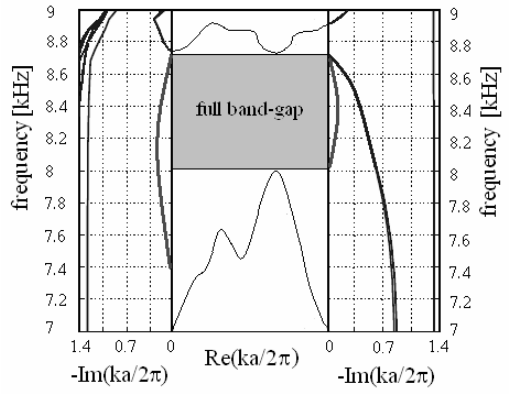

Fig. 7 – Band structure for the panel in the case of Reddy law.

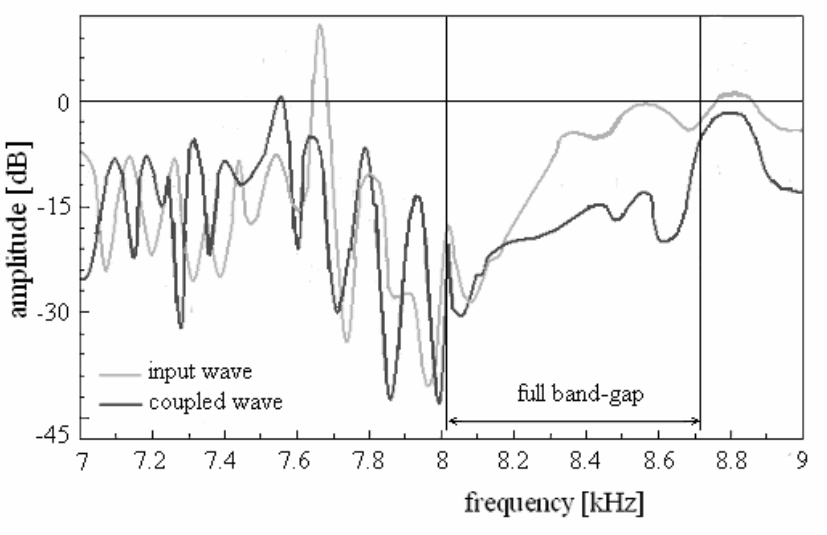

Fig. 8 – The input and coupled waves for panel in the case of Reddy law.

The influence of the diameter size of the hollow sphere is investigated for three values of a, i.e. 0.12m, 0.09 m and 0.08 m with similar wall thickness of 0.00275m and $\xi_0 = 0.3$.

Figures 9–11 show the Insertion Loss spectra of the panel for three sizes of diameter 0.12 m, 0.09 m and 0.08 m respectively. We observed that by increasing the size of diameter, the resonance appears to lower frequency, namely 1.8 kHz, 1.5kHz and 1.1 kHz respectively.

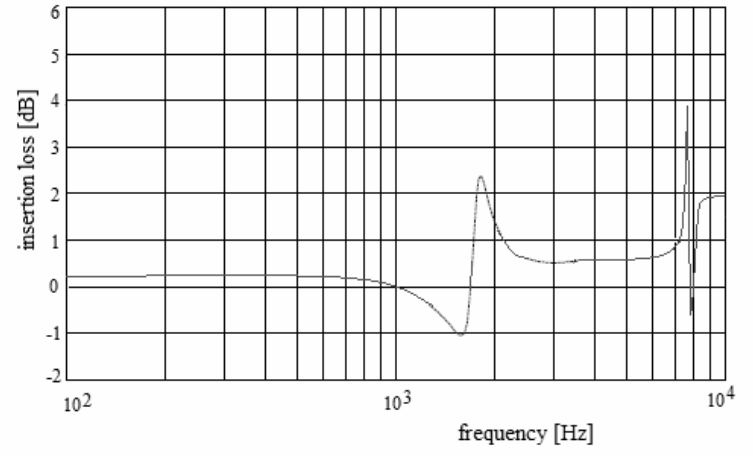

Fig. 9 – Insertion loss spectra of the panel for a diameter 0.12 m.

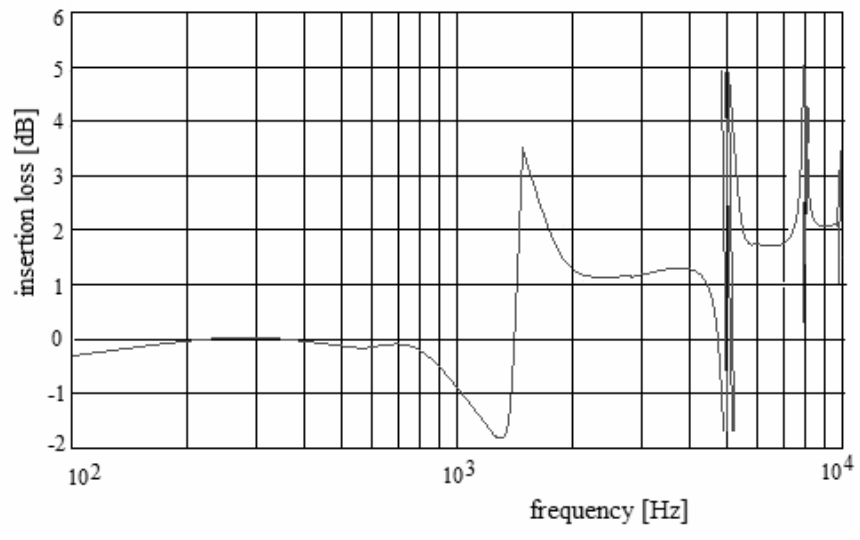

Fig. 10 – Insertion loss spectra of the panel for a diameter 0.09 m.

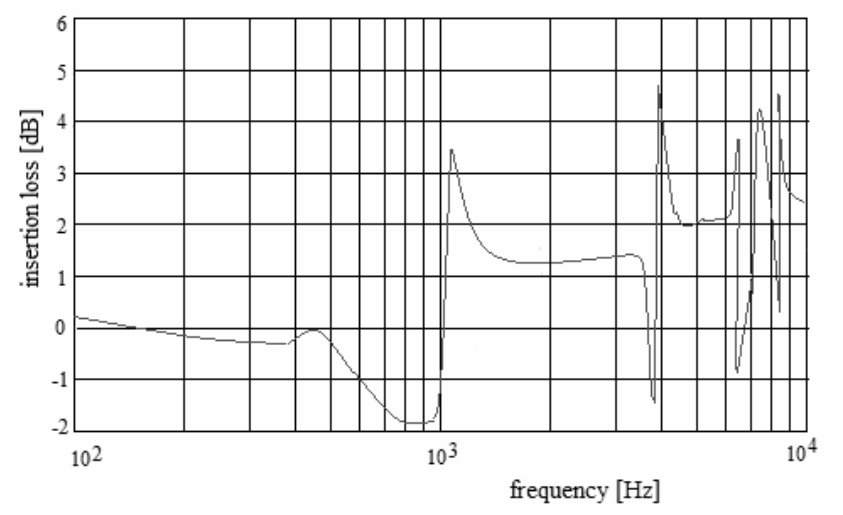

Fig. 11 – Insertion loss spectra of the panel for a diameter 0.08 m.

4. CONCLUSIONS

An alternative noise barrier for the road traffic is reported in this paper using an array of piezoceramic hollow spheres of functionally graded materials - the Reddy graded hollow spheres. The sonic composites exhibit a selective noise attenuation in the band gaps related to the size of the scatterers. The enhancing the

band gaps in the low frequency domain is investigated the intrinsic acoustic properties of the scatterers. We observed that by increasing the size of diameter, the resonance appears to lower frequency, namely 1.8 kHz, 1.5kHz and 1.1 kHz respectively. The results confirmed the existence of the Bragg band gaps for noise barriers and the predicted multiple resonances at frequencies below the first Bragg band gap.

Acknowledgements. This work was supported by the Romanian Academy. The support is gratefully acknowledged.

Received on July 24, 2020

REFERENCES

1. SMITH, B.J., PETER, R.J., OWEN, S., *Acoustics and noise control*, Longman, 1985.
2. BRILLOUIN, L., *Wave propagation in periodic structures*, Dover Publications Inc., 1946.
3. YUNG BOON CHONG, *Sonic Crystal Noise Barriers*, PhD Thesis, The Open University, 2012.
4. MUNTEANU, L., CHIROIU, V., SIRETEANU, T., IOAN, R., *Sonic multilayer composite films*, chapter 11 in Inverse Problems and Computational Mechanics, Vol. 2, Editura Academiei, 2016, pp. 251–170.
5. CHIROIU, V., MUNTEANU, L., DUMITRIU, D., RUGINĂ, C., BRIȘAN, C., *On the sonic films with defects*, Proceedings of the Romanian Academy, series A, **18**, *4*, pp. 378–385, 2017.
6. MUNTEANU, L., CHIROIU, V., SIRETEANU, T., DUMITRIU, D., *A multilayer sonic film*, Journal of Applied Physics, **118**, *16*, 165302, 2015, DOI: 10.1063/1.4933291.
7. HIRSEKORN, M., DELSANTO, P.P., BATRA, N.K, MATIC, P., *Modelling and simulation of acoustic wave propagation in locally resonant sonic materials*, Ultrasonics, **42**, *1–9*, pp. 231–235, 2004, https://doi.org/10.1016/j.ultras.2004.01.014.
8. MUNTEANU, L., CHIROIU, V., *On the dynamics of locally resonant sonic composites*, European Journal of Mechanics-A/Solids, **29**, *5*, pp. 871–878, 2010, DOI:10.1016/j.euromechsol.2010.02.013
9. MUNTEANU, L., *Nanocomposites,* Editura Academiei, 2012.
10. CVETICANIN, L., CVETICANIN, D., *Application of the Acoustic Metamaterial in Engineering: An overview,* Romanian Journal of Mechanics, **2**, *1*, pp. 29–36, 2017.
11. SÁNCHEZ-PÉREZ, J.V., RUBIO, C., MARTÍNEZ-SALA, R. SÁNCHEZ-GRANDIA, R., GÓMEZ, V., *Acoustic barrier based on periodic arrays of scatterers*, Appl. Phys. Lett., **81**, *5240*, 2002, https://doi.org/10.1063/1.1533112.
12. KHELIF, A. CHOUJAA, A., DJAFARI-ROUHANI, B., WILM, M., BALLANDRAS, S., LAUDE, V., *Trapping and guiding of acoustic waves by defect modes in a full-band-gap ultrasonic crystal*, Phys. Rev. B **68**, 214301, 2003.
13. KHELIF, A., WILM, M., LAUDE, V., BALLANDRAS, S., DJAFARI-ROUHANI, B., *Guided elastic waves along a rod defect of a two-dimensional phononic crystal*, Phys. Rev., E **69**, *6*, 067601, 2004.
14. JOANNOPOULUS, J.D., JOHNSON, S.G., WINN, J.N., MEADE, R.D., *Photonic Crystals. Molding the Flow of Light,* Princeton University Press, 2008.
15. ROMERO-GARCÍA, V., SÁNCHEZ-PÉREZ, J.V., GARCIA-RAFFI, L.M., *Evanescent modes in sonic crystals: Complex relation dispersion and supercell approximation*, Journal of Applied Physics, **108**, *4*, pp. 108–113, 2010.
16. RUGINĂ, C., BRATU, P., MOȘNEGUȚU, V., *On the Burgers' equation and application to nonlinear acoustics,* Romanian Journal of Mechanics, **3**, *2*, pp. 37–47, 2019.

17. CHIROIU, V., BRIȘAN, C., GIRIP, I., *On the Dynamic Optimisation of Sonic Composites,* Romanian Journal of Mechanics, **1**, *1*, pp. 13–20, 2016.
18. REDDY, J.N., *A Generalization of Two-Dimensional Theories of Laminated Composite Laminate*, Comm. Appl. Numer. Meth., **3**, pp. 173–180, 1987, https://doi.org/10.1002/cnm.1630030303
19. REDDY, J.N., LIU, C.F., *A higher-order theory for geometrically nonlinear analysis of composite laminates*, NASA Contractor Report 4056, 1987.
20. REDDY, J.N., WANG, C.M., KITIPORNCHAI, S., *Axisymmetric bending of functionally graded circular and annular plates*, Eur. J. Mech., A/Solids **18**, pp. 185–199, 1999, https://doi.org/10.1016/S0997-7538(99)80011-4.
21. Y. DE KLUIZENAAR, JANSSEN, S.A., F.J. VAN LENTHE, MIEDEMA H.M.E., MACKENBACH, J.P., *Long-term road traffic noise exposure is associated with an increase in morning tiredness*, J. Acoust. Soc. Am., **126**, *2*, pp. 626–633, 2009.
22. BABISCH, W.F., BEULE, B., SCHUST, M., KERSTEN, N., ISING, H., *Traffic noise and risk of myocardial infraction*, Epidemiology, **16**, *1*, pp. 33–40, 2005.
23. BABISCH, W.F., *Road traffic noise and cardiovascular risk*, Noise &Health, **10**, *38*, pp. 27–33, 2008.
24. SANCHEZ-PEREZ, J.V., ROMERO-GARCIA, V., ATTENBOROUGH, K., TAHERZADEH, S., CHONG, Y.B., *The influence of the ground on the attenuation properties of sonic crystal barriers*, 2nd Pan-American/Iberian Meeting on Acoustics 2010, Cancun, Mexico, 2010.
25. CHIROIU, V., MUNTEANU, L., *On the free vibrations of a piezoceramic hollow sphere*, Mech. Res. Comm., Elsevier, **34**, *2*, pp. 123–129, 2007, https://doi.org/10.1016/j.mechrescom. 2006.06.011.
26. CHEN, W.Q., *Vibration theory of non-homogeneous, spherically isotropic piezoelastic bodies*, J. Sound Vibr., **229**, pp. 833–860, 2000, https://doi.org/10.1006/jsvi.2000.3022.
27. CHEN, W.Q., WANG, L.Z., LU, Y., *Free vibrations of functionally graded piezoceramic hollow spheres with radial polarization*, J. Sound Vibr., **251**, *1*, pp. 103–114, 2002, https://doi.org/ 10.1006/jsvi.2001.3973.
28. STAN, M., *On the specific parameters of architectural acoustics,* Romanian Journal of Mechanics, **3**, *2*, pp. 3–14, 2019.
29. STAS 9783/1-94 Standard Acoustics in Constructions. The articulation rate (degree of intelligibility) in public auditoriums. Method of determination.